

**A Proposal for the Paul Scherrer Institute π M1 beam line
Studying the Proton “Radius” Puzzle with μp Elastic
Scattering**

J. Arrington,¹ F. Benmokhtar,² E. Brash,² K. Deiters,³ C. Djalali,⁴ L. El Fassi,⁵ E. Fuchey,⁶ S. Gilad,⁷ R. Gilman (Contact person),⁵ R. Gothe,⁴ D. Higinbotham,⁸ Y. Ilieva,⁴ M. Kohl,⁹ G. Kumbartzki,⁵ J. Lichtenstadt,¹⁰ N. Liyanage,¹¹ M. Meziane,¹² Z.-E. Meziani,⁶ K. Myers,⁵ C. Perdrisat,¹³ E. Piasetzsky (Spokesperson),¹⁰ V. Punjabi,¹⁴ R. Ransome,⁵ D. Reggiani,³ A. Richter,¹⁵ G. Ron,¹⁶ A. Sarty,¹⁷ E. Schulte,⁶ S. Strauch,⁴ V. Sulkosky,⁷ A.S. Tadapelli,⁵ and L. Weinstein¹⁸

¹*Argonne National Lab, Argonne, IL, USA*

²*Christopher Newport University, Newport News, Virginia, USA*

³*Paul Scherrer Institut, CH-5232 Villigen, Switzerland*

⁴*University of South Carolina, Columbia, South Carolina, USA*

⁵*Rutgers University, New Brunswick, New Jersey, USA*

⁶*Temple University, Philadelphia, Pennsylvania, USA*

⁷*Massachusetts Institute of Technology, Cambridge, Massachusetts, USA*

⁸*Jefferson Lab, Newport News, Virginia, USA*

⁹*Hampton University, Hampton, Virginia, USA*

¹⁰*Tel Aviv University, Tel Aviv, Israel*

¹¹*University of Virginia, Charlottesville, Virginia, USA*

¹²*Duke University, Durham, North Carolina, USA*

¹³*College of William & Mary, Williamsburg, Virginia, USA*

¹⁴*Norfolk State University, Norfolk, Virginia, USA*

¹⁵*Technical University of Darmstadt, Darmstadt, Germany*

¹⁶*Hebrew University of Jerusalem, Jerusalem, Israel*

¹⁷*St. Mary's University, Halifax, Nova Scotia, Canada*

¹⁸*Old Dominion University, Norfolk, Virginia, USA*

About 1.5 years after the radius of muonic hydrogen was found to be 5σ inconsistent with earlier determinations from atomic hydrogen level transitions and ep elastic scattering, no resolution to the puzzle has been found. We propose to measure $\mu^\pm p$ scattering, which will allow a second determination of the consistency of the μp interaction with the ep interaction. If the μp scattering is consistent with muonic hydrogen measurements but inconsistent with ep scattering measurements, the confirmation of consistency between lepton scattering and Lamb shift measurements but differences between electron- and muon-based measurements of ep and μp systems would provide strong evidence for beyond standard model physics.

BEAM REQUIREMENTS

- *Beam line:* π M1.
- *Beam properties:* Mixed $\pi/\mu/e$ beam. Estimated fluxes of each particle type with 2 mA primary proton beam and full channel momentum acceptance are given in Table I. The π and e numbers are estimated from the π M1 beam website, while the μ numbers are rough guesses based on limited information of beam particle types. Channel acceptance will be limited to keep the rate to no more than about 10 - 15 MHz.

TABLE I. Estimated beam flux.

Momentum (MeV/c)	Polarity	Total Flux (MHz)	π Flux (MHz)	μ Flux (MHz)	e Flux (MHz)
115	+	9	0.6	2	6
153	+	18	8	2	8
210	+	70	60	5	6
115	-	6	0.06	0.2	6
153	-	9	0.8	0.2	8
210	-	12	6	0.5	6

- *Duration of the experiment:* We expect the experiment to last about three years, with about 2 months of tests from late 2012 – early 2013, and about 6 months of production running after equipment is constructed, about late 2014 – mid 2015.
- *Special conditions:* none.
- *Beam time request for the first period after approval:* Two months of tests from late 2012 – early 2013.

Ring μ SR SINQ Injector1 SLS other

Title of Experiment: Studying the Proton "adius" Puzzle with μ p Elastic Scattering

Experiment Number (if known) _____
 Instrument / Beamline _____ / μ M1
 Date of Experiment (if known) from _____ to _____

SAMPLE	name of substance	liquid hydrogen (LH2), carbon and CH2 foils			
TARGET	chemical formula	H2, C, CH2			
	form of material	powder []	liquid [X]	solid [X]	other []
	amount of material	~0.3 g/cm ² in beam for all targets			
	size of material	a few liters of LH2, a few grams of C and CH2			
	container/sealing:	to be determined			
	transport:	by user []	shipped separately []	already at PSI []	
	removed:	by user []	stored at PSI []	disposed off by PSI []	

Toxic no [X] / yes [], specify:
 ingestion [] inhalation [] skin contact [] eye contact []
 other [], specify: _____
 contact person: P. Hasler

Already radioactive:	no [x] yes []	activity:	Bq	isotopes:	IAEA supervision []
Activation expected:	no [] yes [X]	activity:	Bq	isotopes:	IAEA supervision []

Target cells or C will be mildly activated material. contact person: A. Fuchs

Bio. Hazard no [x] / yes [], specify: _____
 contact person: K. Ballmer

Reactive: no [] / yes [x], specify: Hydrogen is potentially flammable
 inflammable: [] explosive: [] corrosive: []
 in contact with: air [] water [] heat [] other: _____
 contact person: P. Hasler

Equipment during transport/experiment/ storage:	contact person	transp.	exp.	storage
magnetic field	Tesla C. Wernli	[]	[]	[]
pressure	kbar, m ³ S. Bondt	[]	[]	[]
heating	K, Watt P. Hasler	[]	[]	[]
cryogenics	K, coolant W. Gloor	[]	[x]	[]
thin window	L. Simons	[]	[x]	[]
X-ray	kV A. Fuchs	[]	[]	[]
laser	, W T. Lippert	[]	[]	[]
high voltage	kV M. Huser	[]	[x]	[]
other:	P. Oggenfuss	[]	[]	[]

Other Safety Aspects: no [] / uncertain [] / yes [x], specify: See proposal.
 contact person: P. Oggenfuss

I confirm that the information above is correct as well as to respect all safety regulations valid for PSI.
 Date: Jan 22, 2012, E-Mail: rgilman@physics.rutgers.edu Signature: _____

INTRODUCTION

The proton radius was thought to be reliably determined to be ≈ 0.88 fm for several years, by atomic hydrogen and ep scattering measurements. The hydrogen atom experiments led, in the 2006 CODATA analysis [1], to $r_p = 0.8768 \pm 0.0069$ fm. The electron-proton scattering analysis led to $r_p = 0.895 \pm 0.018$ fm in the analysis of [2], which discussed the needed Coulomb corrections and choice of an appropriate parameterization to fit form factor data. This situation changed in summer 2010 when a Paul Scherrer Institute (PSI) experiment [3] reported that the radius determined from muonic hydrogen level transitions is 0.842 ± 0.001 fm, about 5σ off from the nearly order of magnitude less precise non-muonic measurements. We refer to this situation as the proton radius puzzle.

The proton radius puzzle is quite possibly more puzzling now than when it first appeared. First, while there have been a number of suggestions of possible resolutions to the puzzle, several appear to be ruled out or severely constrained based on other measurements, and none are generally accepted. Second, two new electron scattering experiments have reported their data along with new analyses of the proton radius, which increase the discrepancy to be greater than 7σ . One experiment was a precise cross section measurement [4] at Mainz that determined ≈ 1400 cross sections in the range $Q^2 = 0.01 \rightarrow 1$ GeV². The Mainz analysis of only their data with a wide range of functional forms led to a proton electric radius of 0.879 ± 0.008 fm. The second experiment [5] at Jefferson Lab measured $\bar{e}p \rightarrow e'\bar{p}$ to determine 1% form factor ratios in the range $Q^2 = 0.3 \rightarrow 0.8$ GeV². A world analysis of data (excluding the Mainz data set) resulted in a radius of 0.870 ± 0.010 fm, consistent with the Mainz electric radius determination – although there were differences in the magnetic radius determination. A partial summary of recent proton radius extractions is shown in Fig. 1.

The proton radius puzzle has attracted wide interest. There are several possible explanations for the puzzle.

- *Beyond standard model physics.* Several articles have appeared that propose possible novel physics that distinguishes μp from ep interactions. At this point we are unaware of any proposed physics that is generally accepted as an explanation. As an example, in [6] the possibility of a new $U(1)_R$ gauge symmetry is discussed, which leads to different μp and ep interactions. A proposed test is enhanced parity violation in μp scattering, orders of magnitude enhanced from the expected parity violation from Z^0 exchange. However, Ref. [7] points out that this model involves a new vector gauge boson with mass around tens of MeV, which could be radiated from muons. The lack of observation of such a boson in, e.g, $K \rightarrow \mu\nu$

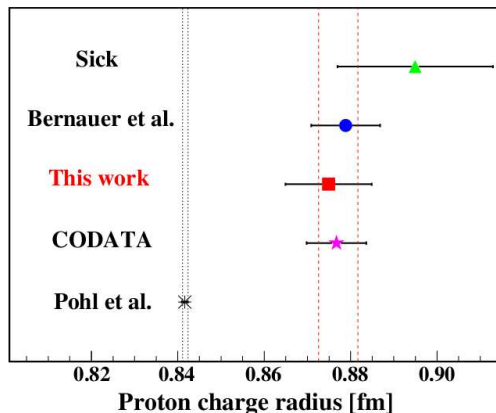


FIG. 1. A summary of some recent proton electric radius determinations, taken from [5].

severely constrains such models. Additional experimental limits on this idea are discussed below.

- *Novel two-photon exchange effects.* When the interaction in the bound atom or in the scattering process involves the exchange of two photons, the intermediate state is an off-shell proton, possibly an excited state of the proton. The relativistic bound state problem remains a difficult and arguably unsolved problem. In [8–10], it was suggested that the two-photon exchange correction has an effect from the proton being off shell, leading to larger corrections in the μp case than in the ep case. The idea is controversial, and it appears at present consistency with other data makes this effect too small to explain the radius puzzle [11].
- *Unexpected aspects of proton structure.* Extracting the radius from the muonic hydrogen Lamb shift requires a proton structure correction. Atomic physics calculations result in $L^{th}(meV) = 209.9779 - 5.2262\langle r_p^2 \rangle + 0.00913\langle r_p^3 \rangle_{(2)}$ where L^{th} is the measured Lamb shift, $\langle r_p^2 \rangle$ is the proton radius, and $\langle r_p^3 \rangle_{(2)}$ is a correction from the third Zemach moment of the proton, given by $\langle r_p^3 \rangle_{(2)} = (48/\pi) \int_0^\infty (dq/q^4)[G_E^2(q) - q^2\langle r_p^2 \rangle/3 - 1]$. The third Zemach moment depends mostly on $G_E(Q^2)$ at low Q^2 . De Rújula [12, 13] suggested that $\langle r_p^3 \rangle_{(2)}$ might be anomalously large. This result is inconsistent with standard fits of the proton electric form factor [14, 15]. This issue was investigated further in [16], which demonstrated that one can add bumps to unmeasured low Q^2 regions of $G_E(Q^2)$ that result in large $\langle r_p^3 \rangle_{(2)}$. Such structures are not predicted by any model of the proton structure of which we are aware. A recent discussion of the atomic physics corrections and their uncertainties is in Ref. [17].
- *Atomic Physics Corrections:* While errors or issues in the atomic physics calculations are in principle a possibility, the radius puzzle has led to a reexamination of the atomic physics that goes into the radius extraction. No significant problems have been found, although there are general critiques of the theory – see, e.g., [18]. At this point, we are unaware of any criticisms of the value of the radius extracted from atomic hydrogen measurements, but there is a criticism that the uncertainty in the radius is not as good as claimed. The essential argument is that many of the atomic physics measurements are correlated, having been done by a few groups. The averaging of these measurements as if they were uncorrelated ignores the issue of correlated techniques and possibly errors. Thus, because of the correlations, the true uncertainty resulting from the atomic hydrogen measurements is not as small as given by the CODATA analysis.
- *Issues in ep Scattering:* The ep scattering data is corrected for radiative, including two-photon, corrections. The conventional radiative corrections are considered to be under control. The two-photon corrections have been an issue in higher Q^2 ep scattering, but all models and all evidence to date is that these corrections become relatively small at low Q^2 . They have been considered at differing level in the analyses of Bernauer *et al.* [4] and Zhan *et al.* [5], and it appears that the uncertainties in these corrections are insufficient to affect the μp vs. ep proton electric radius discrepancy.¹ Once the cross sections are established, the form factors and their slope at $Q^2 = 0$ need to be determined. One can fit Rosenbluth-separated form factors, or the cross sections and any polarization data directly. The use of a functional form might introduce a model dependence. Sick [2] emphasized the use of the continued fraction expansion and a restriction to low- Q^2 data, along with the issues of a conventional Taylor series expansion. Bernauer *et al.* [4] found no significant differences when using a number of functional forms to extract the radius, although they did find that the conventional dipole formula is not consistent with more flexible parameterizations. Paz [18] argued in favor of a constrained z expansion, concluding that the model dependence of other fits leads to an

¹ Issues related to fitting and 2γ corrections have much more effect on extractions of the magnetic form factor and radius at low Q^2 , due to the dominance of the electric form factor in most low Q^2 cross section measurements.

uncertainty about twice as large as reported. He obtained $r_E^p \approx 0.871 \pm 0.01$ fm, consistent with previous ep determinations, but slightly smaller, $\approx 3\sigma$ from the muonic hydrogen result. This fit does not include the recent Mainz and JLab data, or full 2γ exchange corrections. While the radius might be sensitive to the 2γ corrections and parameterization used for the low Q^2 expansion, recent extractions have examined these effects and attempted to include estimates of the corrections and associated uncertainties. The different extractions yield consistent results and find that these effects are significantly smaller than the discrepancy with the muonic hydrogen result.

The differences between the proton radius measured in the μp system and in ep systems is a surprise in part due to universality being generally accepted. Tests of the equivalence of μp and ep systems from a few decades ago provided constraints on violations of and possible differences between the widely accepted universality of ep and μp interactions. We give two examples here.

The radius of ^{12}C is one of the most precisely determined radii from electron scattering. The electron scattering result [19] is $\langle r^2 \rangle^{1/2} = 2.472 \pm 0.015$ fm, based on scattering of 25 – 115 MeV electrons at momentum transfers from 0.1 – 1.0 fm^{-1} , or $Q^2 \approx 0.0004 - 0.04$ GeV^2 . A subsequent analysis of world data [20] found that dispersive corrections increase the extracted radius to 2.478 ± 0.009 fm. Nuclear charge radii were also measured by determining the ≈ 90 keV X-ray energies in muonic carbon atoms to several eV [21]. Assuming a harmonic oscillator nuclear charge distribution led to a ^{12}C radius of $\langle r^2 \rangle^{1/2} = 2.4715 \pm 0.016$ fm. A subsequent muonic atom experiment [22] found $\langle r^2 \rangle^{1/2} = 2.483 \pm 0.002$ fm. There is evidently no μp vs. ep issue in the carbon radius determination. One can question whether one might have opposite effects in the case of μn vs. ep interactions, and whether there might be important corrections – e.g., 2γ effects – omitted from the analyses.

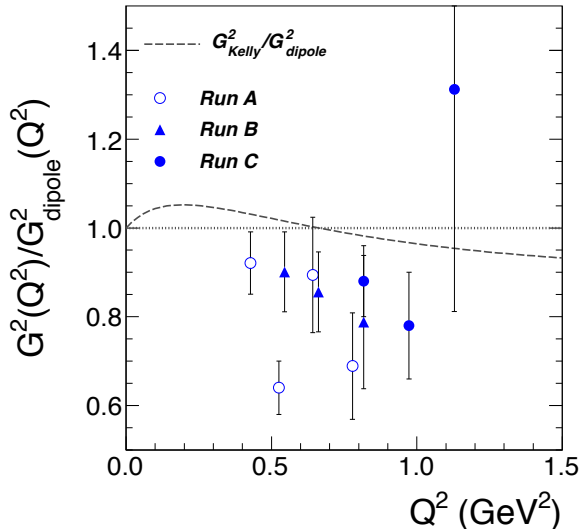


FIG. 2. Reduced cross sections, $d\sigma/d\Omega/d\sigma/d\Omega_{Mott}$, for μp elastic scattering, from Ellsworth *et al.* [23]. The data are somewhat below expectations from the dipole form factor parameterization. Use of the more modern Kelly parameterization [24] does not qualitatively change the result.

One of the better early μp elastic scattering experiments was Ellsworth *et al.* [23], which found that cross sections in the range $Q^2 \approx 0.5 - 1$ GeV^2 were about 15% below the standard dipole parameterization, $G_E = G_M/\mu_p = (1 + Q^2/0.71)^{-2}$ with Q^2 in GeV^2 , and a similar percentage

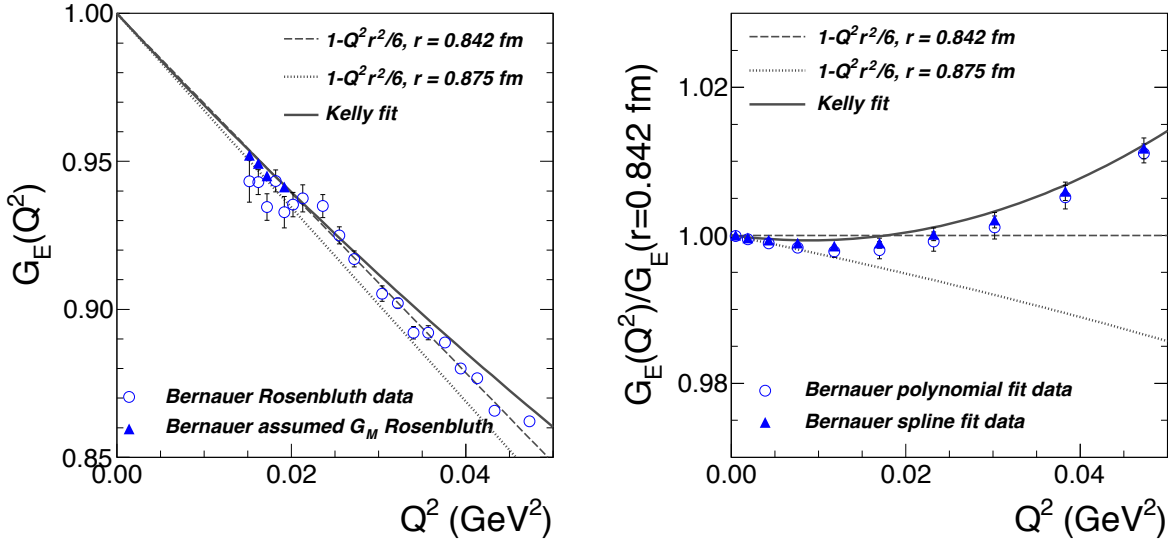


FIG. 3. Left: Mainz result for the proton electric form factor determined by Rosenbluth separations, compared to linear fits assuming two different radii. Right: Mainz results for the proton electric form factor determined by spline and polynomial fit analyses of the cross sections, along with the Kelly parameterization and a linear fit assuming the radius determined by ep measurements, relative to expectations from a linear fit using the radius determined from μp atoms.

below modern form factor fits. as shown in Fig. 2. While this suggests an ep vs. μp interaction difference, Ellsworth *et al.* interpreted the difference as an upper limit on any difference in μp and ep interactions. These data are too high in Q^2 to make any inferences about the proton radius. A subsequent experiment [25] covering $0.15 < Q^2 < 0.85$ GeV² found cross sections about 8% smaller than the electron scattering results, similar to [23], and considered the μp and ep scattering results consistent within uncertainties. A final elastic scattering experiment [26] analyzed the ratio of proton elastic form factors determined in μp and ep scattering as $G_{\mu p}^2/G_{ep}^2 = N(1 + Q^2/\Lambda^2)^{-2}$, with the result that the normalizations are consistent with unity at the level of 10%, and the combined world μp data give $1/\Lambda^2 = 0.051 \pm 0.024$ GeV⁻², about 2.1σ from the electron-muon universality expectation of 0. For deep-inelastic scattering [27], a similar analysis yields a normalization consistent with unity at the level of 4% and $1/\Lambda^2 = 0.006 \pm 0.016$ GeV⁻². In summary, old comparisons of ep and μp elastic scattering have sometimes indicated several percent differences between μp and ep with similar size uncertainties, or sometimes indicated consistency with several percent uncertainties. The constraints on differing μp and ep interactions are not very good. While ep studies have advanced significantly in the past decade, the μp work has not.

Two-photon exchange effects have also been tested in μp scattering. In [28], no evidence was found for 2γ effects, with μ^+p vs. μ^-p elastic scattering cross section asymmetries consistent with 0, with uncertainties from $4 \rightarrow 30\%$, and with no visible nonlinearities in Rosenbluth separations at $Q^2 \approx 0.3$ GeV². The Rosenbluth cross sections were determined to about 4%. Tests in ep scattering [29] have found no nonlinearities even with $\approx 1\%$ cross sections; improved experiments are underway [30].

In ep scattering, the radius is determined from the slope of the form factor at $Q^2 = 0$. Here we consider the Mainz ep data in more detail, as it is related to the measurements that we will propose. Figure 3 shows two indications of the proton radius from the Mainz data set. The left panel shows the Rosenbluth results (open circles) for $G_E^p(Q^2)$ at the lowest Q^2 . The lowest Q^2

extracted values are more consistent with a larger radius than with the muonic hydrogen radius. However the Mainz magnetic radius is found to be smaller than most magnetic radii from other fits. If the magnetic form factor is constrained to be in the region of $1 \rightarrow 1.05$ times the standard dipole, the solid triangle points result. These points are larger than the Rosenbluth values, but still more suggestive of a larger radius. The right panel shows $G_E^p(Q^2)$ extracted from the cross sections using spline and polynomial fit functions to the data. Here one sees that the lowest Q^2 points are more consistent with the larger radius found in ep experiments, but that even before 0.02 GeV² the form factor is starting to show nonlinearities. The Kelly parameterization [24] generally predicts the trends of the data. The curvature at low Q^2 indicates the importance of measuring at low Q^2 to be sensitive to the radius.

Within the ep scattering community, the proton radius puzzle has led to studies about how to push the ep scattering measurements to lower Q^2 , for the possibility that the experiments do not go to low enough Q^2 to see structure that might affect the radius determination from atomic physics measurements, as well as the form factor extrapolation to $Q^2 = 0$. An experimental proposal PR12-11-106 [31] was made to Jefferson Lab PAC39; it was conditionally approved by the PAC, which requested “an updated proposal with final target details, credible simulation of beam requirements including halo and stability, and a well defined path to extend reliability of radiative corrections to Q^2 down to 10^{-4} .” But the JLab PAC considered the measurement of high importance, noting “*Testing of this result is among the most timely and important measurements in physics.*” Based on the JLab 12-GeV upgrade schedule, the experiment is not likely to run until 2016 or so. Studies have also been done of possible future experiments measuring high energy proton scattering on electrons [32], or using an ep collider [33]. However, it should be noted that the atomic hydrogen measurements are at even lower Q^2 than the muonic hydrogen measurements, and ep scattering and atomic hydrogen are consistent.

To summarize the situation, how to resolve the proton radius puzzle remains unclear. The resolution might arise from beyond standard model physics, novel two-photon exchange mechanisms / inadequacies in the theoretical treatment of the bound state problem, unexpected structure in the proton form factors, or issues and / or underestimated uncertainties in the determination of the radius from the actual experimental data. In the ep scattering community, a much discussed possible experimental approach to resolving this puzzle among the data from muonic hydrogen, atomic (ep) hydrogen, and ep elastic scattering is an improved low Q^2 ep elastic measurement.

THE PROPOSED MEASUREMENT

Here, we propose another approach to resolving the proton radius puzzle: measuring elastic μp scattering and making comparisons to ep scattering at the cross section level, with extracted form factors, and ultimately with an extracted radius. The basic idea is that, if the μp and ep interactions are different, this should be reflected in the scattering experiment as well as in the atomic vs muonic hydrogen measurement. This experiment most directly tests the most interesting possible explanations of the proton radius puzzle, that there are differences in the μp and ep interactions. A determination that the μp scattering cross section reflects the radius determined in muonic hydrogen, while the ep scattering reflects the radius determined in atomic hydrogen, would be compelling evidence for beyond standard model physics, a difference in the interactions of the two lepton generations.

If, however, the μp scattering agrees with existing ep scattering, it puts limits on differences between the interactions of the two lepton generations. It is impossible to rule out from experiments narrow structures in the form factors below the minimum Q^2 of the experiment, that lead to incorrect radius extractions from the scattering measurements and corrections in extracting the radius from the atomic physics measurements. However, these proposed measurements along with the proposed JLab measurements [31] will be able to further constrain this possibility by making cross section measurements and extracting the charge form factor at very low Q^2 values.

Beyond proposing simply μp scattering, it is important to measure both $\mu^\pm p$ scattering for a reasonably precise constraint on 2γ exchange effects. As mentioned above, it is now well understood that there is a potentially important 2γ -exchange correction to ep scattering. The 2γ -exchange correction leads to a difference between $\mu^\pm p$ scattering. The correction is believed, based on model calculations and data, to be small for low Q^2 ep scattering. Calculations typically put it at the percent level, while constraints from e^+p to e^-p comparisons are typically limits at the level of a few percent. An interesting feature of this experiment is that the 2γ exchange effect depends not only on Q^2 but also on the scattering angle. The 2γ exchange corrections in theoretical models generally decrease for constant Q^2 as the energy of the beam increases and the scattering angle decreases. Since this experiment runs at lower energy than the experiments running at electron machines, the scattering angle is larger and the 2γ exchange effect might be as well. Thus, this proposal will be unique in having not only μ^\pm but also e^\pm comparisons at large angles and low Q^2 , exactly the region of interest.

Indeed, there is an active program to improve the experimental constraints on 2γ exchange corrections with new measurements at Jefferson Lab [34–36], DESY [37], and Novosibirsk [38]. These measurements are generally intended for the region $Q^2 > 0.5 \text{ GeV}^2$, where polarization and cross section techniques differ significantly in their determination of the form factors. The only recent result published to date [34] is that, at $Q^2 \approx 2 \text{ GeV}^2$, 2γ -exchange effects in polarized ep scattering appear to be small. The recent theoretical idea that ep and μp differences arise from a novel 2γ exchange effect, is controversial, and it presently appears that this mechanism is insufficient to explain the radius puzzle, but the possibility of such an effect can and should be ruled out if one is to make a claim for novel physics.

The experiment requires both high statistics and high precision to limit systematic uncertainties. Even though low- Q^2 cross sections are large, we will not be able to duplicate the statistical precision of the Mainz experiment [4], which operates at much higher luminosity. We should however be able to improve upon their systematic uncertainties. Note that while high absolute precision is desirable, one can in principle rely on high point-to-point precision, if measurements reach sufficiently low Q^2 that one can determine absolute normalization through a fit including the known form factors at $Q^2 = 0$: $G_E^p(Q^2 = 0) = 1$ and $G_M^p(Q^2 = 0) = \mu_p$. This is what was done in the analysis of the Mainz data of Bernauer *et al.* [4]. Our intent is to achieve few tenths of a percent point-to-point uncertainties, to facilitate comparison with the Mainz data, and to allow a precise comparison of μp and ep scattering within this experiment.

For the following discussion, it should be noted that we envision the experiment running in two stages. The first stage is a test measurement with a relatively simple system to check the characteristics of the beam line and our plans for detectors for the experiment. This first stage will include studies of the beam as a function of momentum, and a lower precision test measurement of the scattering cross sections at a beam momentum of $\approx 153 \text{ MeV}/c$. It should be possible to start this stage of the experiment in the last half of 2012. It would involve a few months of setup work along with a few weeks of beam time.

The second stage of the experiment will use the new equipment for production data taking, measurement of the $\mu^\pm p$ elastic cross sections at three beam momenta, $p_{in} \approx 115 \text{ MeV}/c$, $153 \text{ MeV}/c$, and $210 \text{ MeV}/c$. The $e^\pm p$ elastic cross sections will also be measured. We expect that the second stage of the experiment to start in late 2014 or early 2015 and to be done over the course of several months.

To summarize, we expect to:

- determine μp cross sections and form factors for comparison to world ep data
- perform a direct μp to ep comparison in the same experiment
- test 2γ exchange with $\mu^\pm p$, and
- test 2γ exchange with $e^\pm p$.

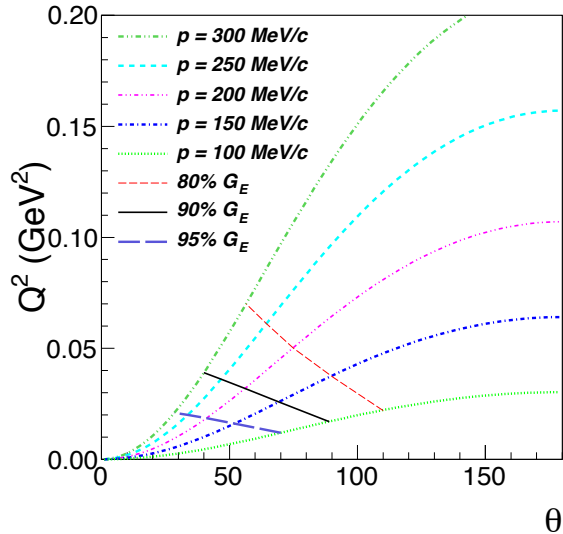


FIG. 4. Q^2 vs. θ for different incident beam momenta. Also shown are lines that indicate where the electric response leads to 80%, 90%, and 95% of the total cross section.

The experiment will study multiple physics issues: basic and novel 2γ exchange effects, lepton flavor universality, proton form factors, and the proton radius.

EXPERIMENTAL DETAILS

Beam and Beamline

Figure 4 gives an overview of the kinematics accessible with PSI beams up to a few hundred MeV/c momentum range. As shown in Fig. 3, one can distinguish a larger or smaller radius from precise cross sections that go no higher than about 0.04 GeV^2 , and by this momentum transfer terms beyond the leading-order radius term clearly affect the cross section. One needs beams of up to about $150 \text{ MeV}/c$ to obtain this four-momentum transfer. With PSI muon beams up to momenta of about $200 \text{ MeV}/c$, one can cover this range of Q^2 in kinematics in which the electric response dominates the cross section, at the level of 80% or more. The estimates in Fig. 4 are based on the Kelly form factor parameterization [24]. Covering a range of energies and angles also allows sensitivity to the magnetic response, through a Rosenbluth separation or through a form factor fit.

We propose a program of measurements in the πM1 beamline of PSI. The πM1 beamline, most extensively described in [39], has a nominal momentum range of about $110 - 560 \text{ MeV}/c$. Figures 5 and 6 shows some beam line properties. For negative polarity at $270 \text{ MeV}/c$, the $e^- : \mu^- : \pi^-$ fractions are $12\% : 1.3\% : 86.5\%$, with the μ^- flux $\approx 10^5 \text{ mA}^{-1}\text{s}^{-1}$. For positive polarity at $165 \text{ MeV}/c$, the $e^+ : \mu^+ : \pi^+$ fractions are $29\% : 15\% : 56\%$, with the μ^+ flux $\approx 10^6 \text{ mA}^{-1}\text{s}^{-1}$. The π flux peaks at higher momenta, while the μ and e fluxes peak at lower momenta. Because of the decreasing μ flux at higher momenta, measurements much above $200 \text{ MeV}/c$ would be quite challenging. The μ fraction appears to have not been well characterized. It appears that the μ^+ flux is a few MHz/mA of primary proton beam for μ^+ in the momenta range of interest, but

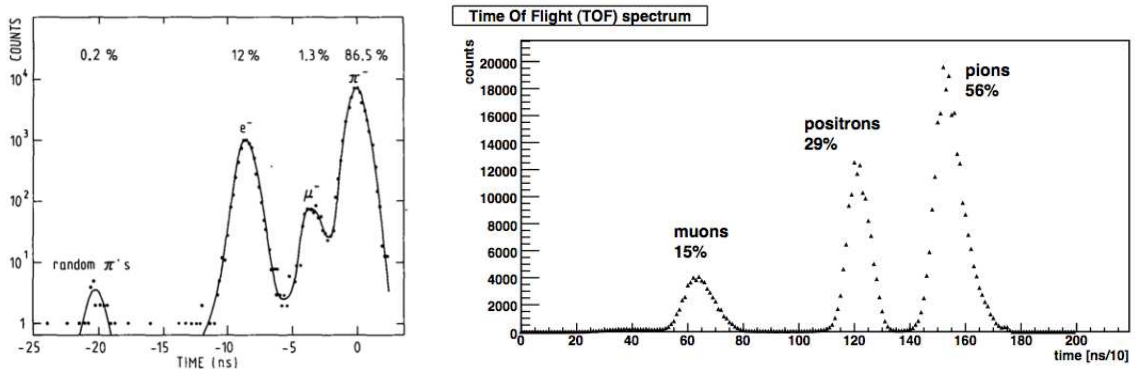


FIG. 5. Left: Time of flight spectrum for negative polarity beam particles for 270 MeV/c beam, from [39]. Right: Time of flight spectrum for positive polarity beam particles for 165 MeV/c beam, from [40].

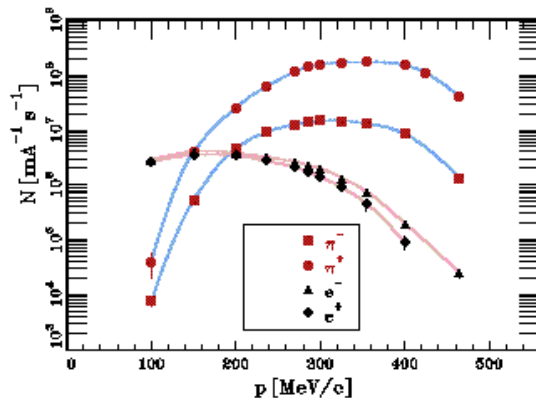


FIG. 6. Electron and pion fluxes for the π M1 beamline as a function of momentum, for a 2.9% (FWHM) momentum acceptance, from the PSI website [41]. The fluxes are particles per second for 1 mA of primary proton beam current into the π production target. Typically the primary proton beam current is 2 mA. Experiments have used momentum acceptances at least as small as 0.1% [40].

several times smaller for μ^- . This flux leads to $\approx 10^{11}$ ($\approx 10^{10}$) incident μ^+ (μ^-) per day at a single incident energy.

The obvious issue related to the beamline is the question of whether it is possible to measure precise μp elastic cross sections with large π and e backgrounds in the beam. Fig. 5 indicates that beam TOF measurements can sufficiently cleanly distinguish μ from e from π , at least if the μ fraction is not too small. Simultaneous measurement of the ep and μp scattering reduces systematics in comparing the cross sections and form factors, if the beam particle types can be isolated, and the combined rates can be handled. Figure 7 shows the timing for the various particle types relative to the beam RF time, as a function of momentum, calculated 21.3 m from the production target, outside the shielding wall and inside the π M1 area. It can be seen that the particle RF times are well separated at some beam momenta, but coincide at others.

The right panel of Fig. 7 shows the minimum time difference for each particle type from the other two. If the particles are within an RF bucket in the order, for example, e , μ , and π , then the e has some time separation $t_{\pi e}$ from the π in the preceding RF bucket and a separation $t_{e\mu}$ from

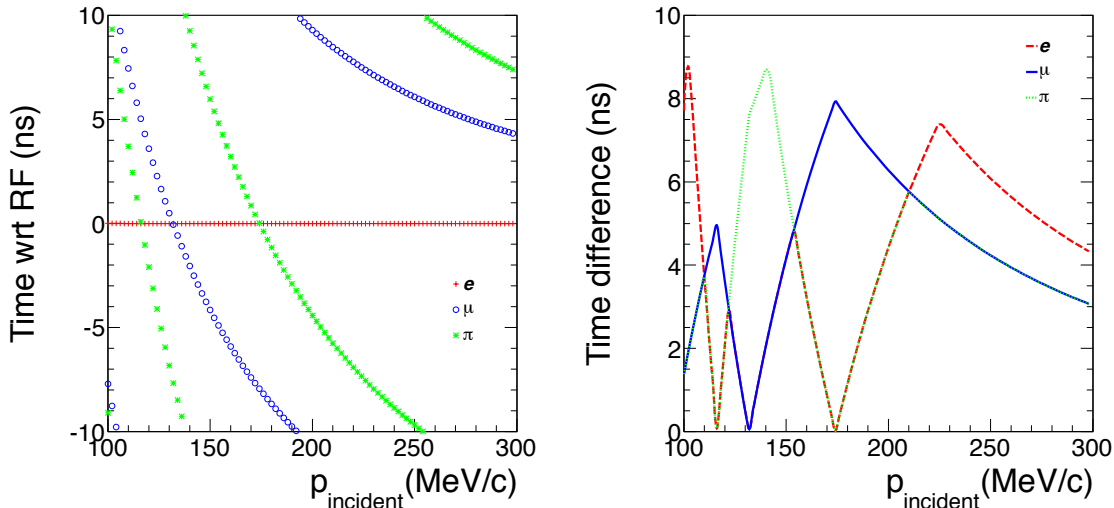


FIG. 7. Left: Time of flight for e 's, μ 's, and π 's relative to beam RF time. With the 50 MHz structure of the beam RF time has a 20 ns range, shown here as -10 to 10 ns. Because the electrons have $\beta = 1$ across the momentum range, their time is fixed relative to the beam RF, and they are graphed here at $t = 0$. Right: Minimum separation between the RF times of the three particle types. For each particle there are two RF time separations, to the other two particles, and the shorter of these two times is shown. Thus the plot always has two overlapping minimum time difference curves, since two particles are closest together and one larger time difference curve, except for four points where one particle is midway between the other two. The brown curve results with the e and π have the same minimum separation time. The three particle types are best separated with RF timing near 210 and 150 MeV/c.

the following μ in the same RF bucket. The μ follows the electron by $t_{e\mu}$ and precedes the π by $t_{\mu\pi}$. The π follows the μ by $t_{\mu\pi}$ and precedes the e in the following RF bucket by $t_{\pi e}$. Thus, there are only three separation times. If one plots the minimum separation time for all particle types, one has either the case that at least two of the three times are equal and smallest, in which case all particles have the same minimum separation time, or that one of the three times is smallest, in which case two particles share the same minimum separation time, and one has a larger minimum separation time.

Figure 7 shows, for example, that each particle type is at least 4 ns apart from both other particle types for momenta from $149 \rightarrow 157$ MeV/c and from $197 \rightarrow 258$ MeV/c. In these ranges it should be possible to measure both μp and $e p$ scattering with clean beam PID. For the range $111 \rightarrow 119$ MeV/c it is possible to cleanly distinguish μ 's, but the π and e RF times cross and these particles cannot be separated. Thus at 115 MeV/c we only plan to measure $\mu^{\pm} p$ scattering. Our judgment is that it will be sufficient to run this experiment at these three momenta settings, $p_{in} \approx 115$ MeV/c, 153 MeV/c, and 210 MeV/c with a mixed $\pi+\mu+e$ beam. It will not be necessary to operate at other momenta, either for redundancy or to obtain a wider range of kinematic settings, or to have a clean beam to reduce detector rates this will be discussed further below.

An additional concern is the sensitivity of the measurement to the beam properties. Figure 8 shows the sensitivity of the cross section measurement to the beam momentum. An offset in momentum leads to a roughly constant shift in the cross section, with little angle dependence, except for backward angles at low momentum. Since the cross section depends on the form factors squared, effects on the form factors are half as large as on the cross section – the $\approx 0.05\%$ point-to-point variations become 0.025% in the form factors, and the 0.1 - 0.2% overall changes become

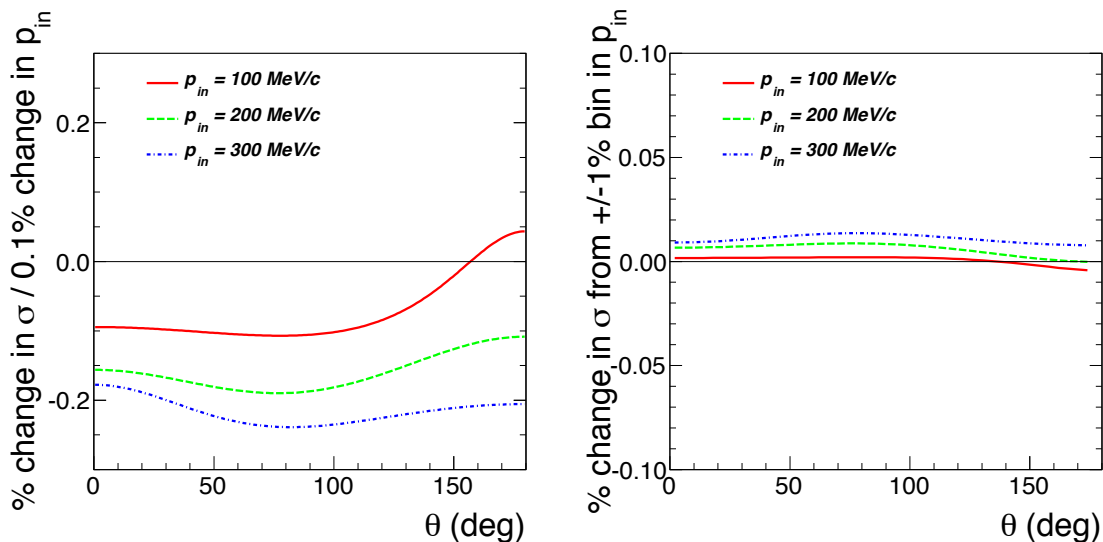


FIG. 8. Left: sensitivity of the cross section to changes in the beam momentum. Right: effect of averaging the cross section over a $\pm 1\%$ momentum bin.

0.05 - 0.1% absolute uncertainties in the form factors. This uncertainty is tolerable. Thus, knowing the beam momentum to 0.1% is sufficient.

Figure 8 also shows that the determination of the cross section is relatively insensitive to averaging over a $\pm 1\%$ momentum bin, but this result is based on the flux being independent of momentum, and the central momentum being well known. Since the flux can vary strongly with momentum, as shown in Fig. 6, it is important to either limit the channel momentum acceptance or to determine the flux as a function of momentum so that the appropriate averaging can be done. The π M1 channel nominal momentum resolution is about 0.1%, but the channel with the fluxes we quoted is operated with $\approx 3\%$ momentum acceptance. The momentum distribution can be determined either by operating the channel momentum dispersed on the target, or by measuring the momentum of each incoming particle. As described in [39], the π M1 channel was operated with an intermediate focal point between the dipole magnets where the dispersion was ≈ 7 cm/%. A wire chamber with 1-mm resolution placed at the focus determined momenta to 0.03% (FWHM). Operating the channel in this mode should allow maximum flux with a large momentum bite, while keeping the beam energy systematic shown in Fig. 8 under control, much better than is needed.

The π M1 web pages [41] give a spot size on target of 1.5 cm horizontal by 1 cm vertical, with angular divergence of 35 mr horizontal by 75 mr vertical. (Alternate beam tunes are possible, and we are working towards assessing whether the experiment would be improved with a different beam tune.) But offsets in the scattering angle need to be determined at the \approx mr level, as shown in Fig. 9, and scattering angles of individual events need to be determined at the several mr level, as shown in Fig. 10. This level of precision cannot be achieved without measuring incident particle trajectories due to the large angular divergence of the beam, 35 mr horizontal by 75 mr vertical. Thus, beam chambers are needed to measure the incident beam trajectory on an event by event basis.

Finally, it is necessary to determine the beam flux precisely to measure a precise cross section. The most straightforward way to do this is to count the beam particles, if the flux is not too large for the detectors.

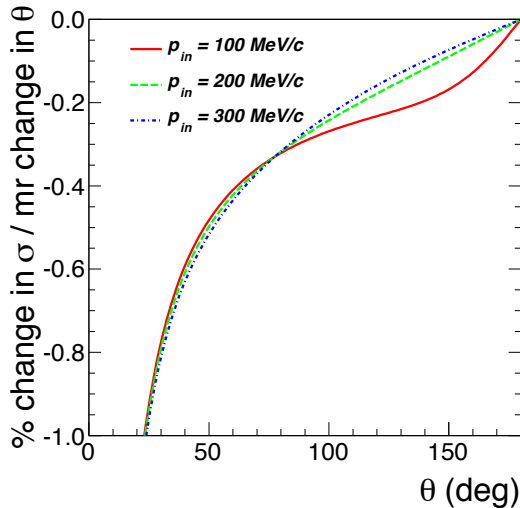


FIG. 9. Sensitivity of the cross section to changes in the scattering angle. The increasing systematic uncertainty at small angles from offsets is one of several reasons cross section measurements will be limited to about $20^\circ < \theta < 100^\circ$.

Beam Line Detector Plans

The beam line detectors have to operate at high rates, ≈ 10 MHz, determine the beam momentum, determine trajectories into the target at the few mr level, and count the number of π , μ , and e beam particles. These tasks can be accomplished with a system of GEM chambers and scintillating-fiber (sci-fi) arrays. The GEM chambers have resolution < 0.1 mm (σ) and rate capability of tens of MHz/cm² with pixel readout. Although Monte Carlo studies indicate that multiple events through the chambers 30-50 ns apart can be resolved, it is usually assumed that the GEM chamber readout will integrate over all tracks within a ≈ 250 ns window. The sci-fi detectors will use 2-mm square fibers. Muons passing through the fibers will lose about 0.5 MeV and generate about 70 photons at the readout end of the fiber. The energy loss and number of photons generated are about twice as large for electrons. At this point we are considering using Multi-Pixel Photon Counters (MPPCs) for readout. MPPCs have a gain of order 10^6 , high quantum efficiency, an intrinsic time resolution of about 0.2 ns (σ), and are insensitive to magnetic fields.

The beam momentum will be determined at the intermediate focal point in the channel. With the dispersion at the focus of 7 cm/%, the position only needs to be determined to a few mm. Coupled with the requirement of a 10 MHz rate of beam particles, we choose the faster sci-fi array to determine the beam momentum. Within any RF bucket there is only a $\approx 20\%$ chance of a second particle. The sci-fi array will have about 21 cm / 2 mm = 110 elements, so rates in each fiber are small, and second particles are rarely in the same element. Since the beam is mostly π 's and e 's, the background particle is rarely a μ . At the position of the intermediate focal point, the RF time separations of the different particle times are always greater than 3.5 ns, so the sci-fi counter should be able to efficiently identify μ 's and determine their momenta even at high rates. For e 's, due to the higher beam rate, it is not a significant problem to throw out of the analysis $\approx 20\%$ of the events with triggering plus background beam electrons, where it is ambiguous which of two measured momenta is correct.

At low rates, 2 GEM chambers 10 cm apart determine the trajectory into the target on an event by event basis to $\approx \sqrt{2} \times 0.1/100 = \sqrt{2}$ mr, better than is needed. But efficiencies are typically

about 98%, so a redundant third chamber is desirable. Also, at high rates, random background trajectories lead to problems. Due to the large divergence of the beam, $\approx 35 \text{ mr} \times 75 \text{ mr}$, a hit at any point in either GEM chamber could in principle have come from about half of the beam spot on the other chamber - we assume here the position within the beam spot and angles are uncorrelated, and uncorrelated with the momentum, the worst-case assumption. With 10 MHz rates and 2.5 background tracks in 250 ns, there will be typically 3-4 hits in each chamber and 6-8 potential real tracks - one real, 3-4 random, and 3-4 ghost tracks. Having a third chamber generally eliminates the ghost tracks. The background random coincidence tracks can be reduced about 80% by requiring that the trajectory of the beam particle into the target intersects the trajectory of the scattered particle exiting the target. The trajectories in the transverse directions are known to $\approx 1 \text{ mm}$, compared to the $1 \times 1.5 \text{ cm}^2$ beam spot. As described, with 3 GEM chambers at high rates, there is about a 50% chance of a second random coincidence track in an event that cannot be cleanly eliminated. This would lead to a large loss of events at the analysis stage.

To reduce the loss of events at the analysis stage, we plan to add a sci-fi array near the target. The sci-fi array will consist of 3 planes of 2-mm square fibers in an XYU configuration, for higher efficiency along with some redundancy. A sci-fi array before the target can reduce the loss of events by $> 90\%$, in addition to providing a count of the incident flux near the target. (Note that the sci-fi array at the channel intermediate focal point is also counting the beam flux.) The resolution of the array allows it to generate a time for nearly all GEM chamber tracks, eliminating the $> 90\%$ of the events that come from different RF buckets, and those from the same RF bucket that are different particle types than the scattered particle that generated the trigger.

We are also considering whether to add a sci-fi array downstream of the target. While being downstream of the target is counter-intuitive, beam particles will generally go through the target with only $\approx 10 \text{ mr}$ multiple scattering, so the sci-fi should still be able to veto trajectories that pass through the target unscattered, eliminate particles that come from different beam RF buckets and particles of different types than the triggering particle that are in the same RF bucket, and count the beam particles, while not affecting the beam upstream of the target. The first feature, detecting unscattered particles, is an independent measurement which would further enhance the ability to cleanly determine the incoming track at high rates.

UVA already has two existing GEM chambers that are consistent with our requirements. The small GEM chambers are relatively inexpensive, costing only of the order of \$10,000, so it is relatively inexpensive to construct additional chambers.

One issue with the proposed system is the need to separate the different particle types by RF time at the hardware level so that the flux of incident particles can be counted. We have started the conceptual design of an FPGA-based scaler + trigger system. It would take RF signal and scintillator inputs and provide distinct output signals for each of the 3 beam particle types to be used as input to the trigger. It would act as a scaler to be read out so that the number of particles could be counted; we expect to subdivide the 50 MHz beam into 16 time channels, each of width slightly over 1 ns, so that as a scaler we would measure counts vs. RF time. For output to the trigger, the module would have programmable windows to use for the different beam momenta settings.

The beam particle identification system relies solely on RF timing. It would be desirable to have a redundant particle identification system to check the performance of the RF time measurement. Such a system is already available through the $\approx 10 \text{ m}$ flight path between the channel intermediate focal point sci-fi and triggering scintillators, which gives about 3 - 7 ns separation between μ 's and π 's, and a larger separation between μ 's and e 's. Still, it would be desirable to have a Cerenkov counter downstream of the target to identify particles that did not scatter in the target. This system would sample events to check the efficiency of the RF time particle identification. As the RF time identification and whether a particle scatters are uncorrelated - of course different particle types have different interaction cross sections - this system cross checks the particle identification in the scattering data. The system would have a separate trigger and be read out on a highly prescaled basis so that it does not affect the computer dead time.

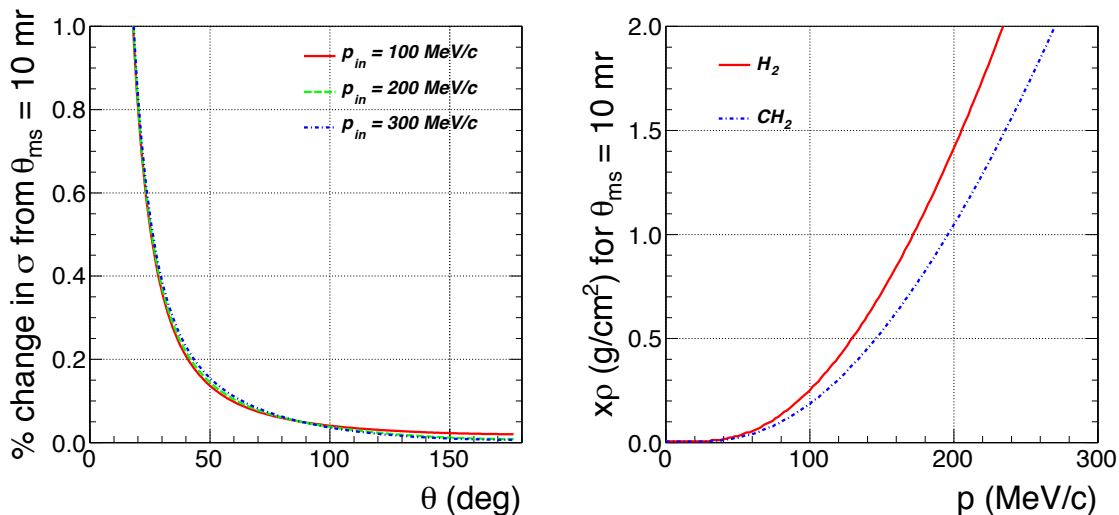


FIG. 10. Left: Effect of multiple scattering on measured cross sections. The increasing systematic uncertainty at small angles from multiple scattering is one of several reasons cross section measurements will be limited to about $20^\circ < \theta < 100^\circ$. Right: Thickness of CH_2 or liquid hydrogen targets leading to 10 mr multiple scattering, as a function of momentum.

To summarize, a study of the systematic uncertainties associated with the beam indicates that it is possible to run the experiment with a mixed e , μ and π beam with properties measured by a set of detectors. A sci-fi array at the channel intermediate focal point determines the beam momentum. Three GEM chambers determine tracks into the target, eliminating ghosts. A sci-fi array near the target removes tracks from other beam RF buckets and other particle types from the same RF bucket. Intersection with the scattered particle trajectory further reduces backgrounds. Redundant particle identification checks will be performed with a Cerenkov counter downstream of the target.

Target

Two common techniques for hydrogen targets are the use of liquid hydrogen targets and the use of hydrogen in a plastic, such as CH_2 or scintillator, along with a carbon target for background subtraction. The main concerns related to the target are multiple scattering and energy loss, which limit the possible target thickness.

Because of the sharp drop of the cross section with angle, multiple scattering, primarily in the target, affects the measured cross section. An estimate of this effect is shown in Fig. 10. The effect is insensitive to energy, with large sensitivity at forward angles due to the sharp drop of the Mott cross section with angle near 0° . For forward angles the multiple scattering needs to be limited to a few mr, or the cross sections need to be corrected for this effect. Keeping multiple scattering small particularly limits the target thickness for the 115 MeV/c setting, to about 0.3 g/cm². One can see from Fig. 10 that the target will have about 10 times more hydrogen in it for equivalent multiple scattering effect if cryogenic hydrogen is used rather than CH_2 , which makes liquid hydrogen the preferred target, as it reduces the needed beam time by an order of magnitude. Since multiple scattering can be reasonably well estimated, it is possible to unfold the multiple scattering from the measured cross sections to determine the form factors.

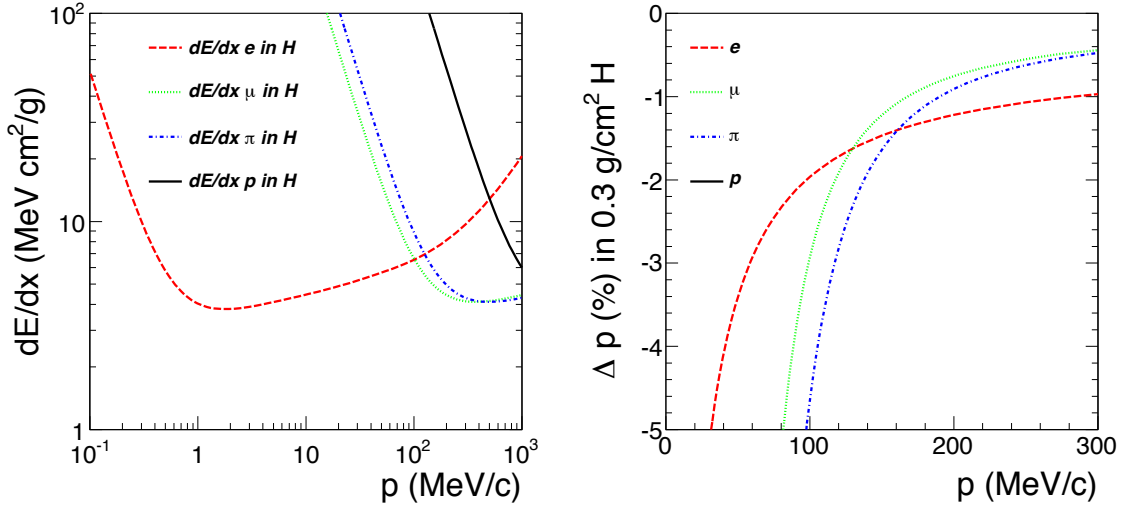


FIG. 11. Left: dE/dx in hydrogen. Right: Change in momentum for particles passing through a 0.3 g/cm² hydrogen target. Protons lose a large fraction of their energy and are off scale.

Because of energy loss in the target, the beam momentum changes as the beam passes through the target. Figure 11 shows dE/dx for the π 's, μ 's and e 's in the beam, along with the energy loss for these particles passing through a target of thickness 0.3 g/cm². The energy losses were taken from NIST ESTAR [42] for the electrons and NIST PSTAR [43] for protons. For μ 's and π 's, dE/dx was set to the proton dE/dx at the same $\beta\gamma$. For μ 's in the momentum range of interest the momentum drop is about 1% – 2%, much larger than our required momentum knowledge of $\approx 0.1\%$, but not a problem based on the estimates of averaging over the beam momentum shown in Fig. 8, since the energy loss and the average interaction momentum can be calculated reliably. For a foil target, the correction relies entirely on the calculated energy loss. For a liquid hydrogen target, a 0.3 g/cm² target is about 4 cm long, and the interaction position can be determined to about 1 mm. This will allow the energy loss correction as a function of distance and energy loss to be studied, providing a valuable cross check.

At present, there does not appear to be an available LH₂ target at PSI. A low-luminosity target with basically the needed functionality has recently been constructed by the Michigan and Maryland groups for use in the Fermilab E906 Drell-Yan experiment. This target could not simply be moved to PSI as E906 is scheduled to be taking data over the next ≈ 3 years, and as the target cells are much longer than desired for a low energy μp experiment. But it provides a guide to the scale of effort and funding needed to construct a similar system from scratch for PSI: about 2 person-years of effort and US \$300,000 [44].

To summarize, a cryogenic target of about 4 cm long maximizes the hydrogen thickness consistent with the needed systematic uncertainties at the lowest beam momentum setting. A second longer cell can be used for higher momentum settings. Given the greater desirability but larger cost and longer time to construct an LH₂ target vs CH₂ and C foil targets, we plan to use the foil targets for the initial set of test measurements, until an LH₂ target is ready for operation.

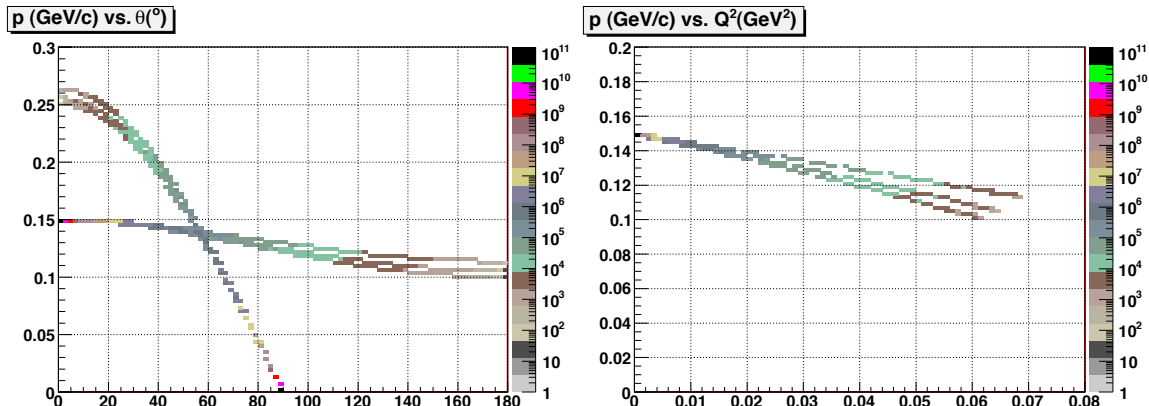


FIG. 12. Left: Curves of p vs θ_{lab} for elastic scattering of 150 MeV/c π 's, μ 's, and e 's from protons. With very similar kinematics and at this resolution the lines are overlapping and largely indistinguishable. The recoil proton lines reach from about 0.25 GeV/c at $\theta = 0^\circ$ out to 90° , while the scattered beam particles only vary from about 0.15 GeV/c to 0.1 GeV/c. At larger angles the differences of $p_e > p_\mu > p_\pi$ can be seen. The differences in the recoil protons near 0° can also be seen. Right: curves of p vs. Q^2 for elastic scattering of 150 MeV/c π 's, μ 's, and e 's from protons. The upper curve is for e 's and the lower curve is for π 's. The recoil protons are not shown.

Detection of Scattered Particles

From the preceding discussion, it is apparent that the detector system needs to have a well determined solid angle and well determined central angles, although measurements on an event by event basis only need to be at the few mr level. It is also clear that we need to cleanly identify and trigger on scattered μ 's and e 's to determine their cross sections, and identify but not trigger on π 's. We now focus on what the scattered particle distributions will be.

When a low energy beam of π 's, μ 's, and e 's impinges in an idealized experiment upon a proton target, no inelastic processes are kinematically allowed, so only elastic scattering is possible until pion production threshold – corrections to this picture are discussed below. Pion production threshold occurs at beam momenta of about 280 MeV/c for π 's, 250 MeV/c for μ 's, and 150 MeV/c for e 's. Thus it is largely not a concern for most of the energy range discussed here, and we do not consider it further.

This idealized situation is reflected in Fig. 12, which shows the kinematics for scattering on protons. The kinematics for the scattered particle and for the recoiling proton are similar for all beam particles. The momenta of scattered π 's, μ 's, and e 's change slowly with angle, and are similar at the same angle. The recoiling proton momentum exceeds the beam momentum at forward angles, and drops to 0 by 90° – the proton cannot be scattered backward of 90° .

One complication to the simple picture is that the beam also interacts with the atomic electrons. The heavy μ 's and π 's scatter from the atomic electrons, losing energy, undergoing multiple scattering, and producing knockout electrons or δ rays. Figures 13 shows the the beam particles basically go forward with little change in their momentum vector, but they produce low momentum, few MeV/c electrons that go out over a range of angles. Because the μ 's and π 's go forward, they do not lead to triggers, and are not a concern. The beam positrons (electrons) undergo Bhabha (Moller) scattering with the atomic electrons, producing high momentum particles for small angles, forward of about 15° , but only few MeV/c particles for larger angles. The high rate of higher momentum e 's in the forward direction are another reason why we limit our planned angle range to about $20^\circ < \theta < 100^\circ$.

A second complication to the simple picture is radiative corrections. In the peaking approxima-

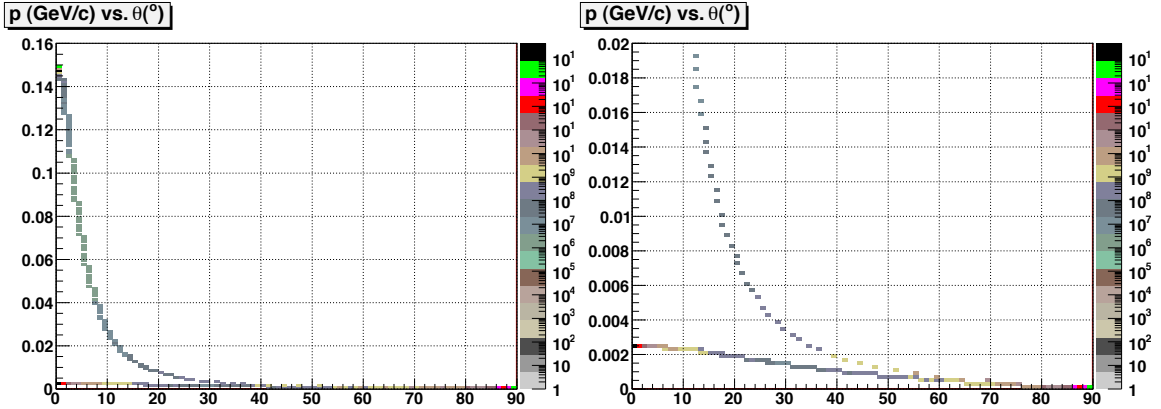


FIG. 13. Scattering of 150 MeV/c π 's, μ 's, and e 's from electrons. The panels are the same, except the vertical scale is expanded for the right panel. For π 's and μ 's, the much heavier beam particle goes forward at nearly the beam momentum, while the recoil electron goes out over a range of angles at very low momentum, a few MeV/c. For an incident e^+ (e^-), there is Bhabha (Moller) scattering, leading to electrons with 10 MeV/c or larger up to about 15° .

tion, an electron can radiate a photon in the beam direction before scattering, or in the scattered direction after scattering. The result of these processes is to remove electron flux from the beam or scattered electrons from being detected, so that the actual “Born” cross section is larger than the experimentally measured cross section. At the kinematics of this measurement, the radiative correction, $\sigma_{Born} = \sigma_{experiment}/(1 - \delta)$, is typically about $1 - \delta_e \approx 85\%$ – the Born cross section is about 15% larger than the experimental measurement. We have done an initial estimate of the radiative corrections for muons by replacing the electron mass with the muon mass in an existing radiative correction code. This reduces the radiative correction about a factor of four ($1 - \delta_\mu \approx 96\%$). We are however rechecking the code. Since it was developed for ultra-relativistic electrons, it might include approximations that no longer apply for the muon in these kinematics, and that, when removed, reduce the corrections further.

The detector system in the range of about $20^\circ < \theta < 100^\circ$ will have similar rates of e 's and μ 's that scatter from protons, with momenta of 100 - 200 MeV/c. We need to track, identify, and generate triggers from these particles. There will be a higher rate of similar momentum π 's, because there is the strong interaction in addition to the electromagnetic interaction, that we need to identify so that π triggers can be suppressed. There will also be a large rate of low momentum, <10 MeV/c electrons from scattering from atomic electrons that should not generate triggers. Finally, there will be a small rate of recoil protons that escape from the target into the region of the detectors; the rate of these protons is sufficiently small that we neglect further consideration of them.

The rate of Moller (or Bhabha) scattering off electrons in the target is a potential concern. The low momentum electrons shown in Fig. 13 will add background hits to the wire chambers without triggering the data acquisition. Figure 11 shows that low momentum e 's are strongly absorbed in the target. Thus, we consider the rates of e 's with momenta above 0.1 MeV/c going into the detector stack. The Moller cross section diverges at 0° and 180° in the c.m. Since $\theta_{cm} = 90^\circ$ corresponds to $\theta_{lab} = 4^\circ - 5^\circ$ in our kinematics, the Moller rate is low in the detectors once a low momentum cutoff is taken into account. We find that the total rate is a few tens of kHz at all beam momenta for our angle range of $20^\circ < \theta < 100^\circ$ with the constraint $p > 0.1$ MeV/c. Much of this rate is near $\theta_{lab} = 90^\circ$ – the rate from 20° to 70° is of order 1 kHz, and the rate from 20° to 80° is around 10 kHz. Thus, Moller and Bhabha scattering off the atomic electrons is not a significant issue. (A GEANT study has been started so that we can include the effects of rescattering of the

electrons as they pass through the target.)

Multiple scattering in the target is a significant effect, limiting the angle reconstruction to ≈ 10 mr. The correction to the cross section arising from the 10 mr multiple scattering is small enough that it can be corrected for reliably, but we need to ensure that the total resolution does not become significantly larger. Thus, it is necessary to minimize additional multiple scattering by having the wire chambers as the first detector element and by ensuring that the wire chamber trajectory resolution is well below the intrinsic 10 mr limit. While on an event by event basis the trajectory only needs to be determined to a few mr resolution so that the chamber resolution does not significantly add to the multiple scattering, the chamber positioning must be precise enough that the scattering angle offsets are below 1 mr.

In summary:

- Detectors covering an angle range of about $20^\circ - 100^\circ$. The forward angle is limited by considerations of high rates and increasingly difficult systematic uncertainties. The largest angle covered is limited by the lack of scattering rate at large angles. To obtain excellent statistics, we are also aiming for an azimuthal coverage of 50% of 2π .
- Good angle resolution requires the initial detector stack element to be a wire chamber. Background singles rate are small.
- Efficient triggering with well measured efficiencies requires multiple scintillator layers with a loose trigger.
- While low energy electrons are ranged out so that they do not lead to triggers, there is a large rate of potential triggers from scattered π 's that must be suppressed at the trigger level.
- Due to the lack of inelastic processes at lower energy, combined with manageable background rates – see below – we find that there is little benefit from using a magnetic field to either momentum analyze scattered particles or to shield the detectors from the high rate of low-energy electrons. Not having a magnetic field should simplify the “optics” of the experiment and make precise cross sections easier.

Precise cross section measurements are traditionally done with small solid angle detectors, adjusting their angle and using luminosity monitors to help determine relative normalizations. This is the technique used in the Mainz ep experiment. While we are confident that such a technique would work here, the low luminosity makes the measurement of a range of angles prohibitive time-wise. We plan instead to construct and precisely position large solid angle detectors with the needed systematic precision.

Spectrometer Detectors

Our plan for the experimental configuration is shown in Fig. 14. The “spectrometer” for the scattered particles consists of wire chambers, Cerenkov counters, and trigger scintillators.

As indicated above, rates are small in the wire chambers. A chamber with 250 ns resolving time and a 30 kHz rate has random tracks in fewer than 1% of events. The background rate is largely low energy, large angle electrons that do not lead to triggers. At the analysis level, it should generally be possible to remove the background tracks using rough positions determined by the scintillators – see below. The key issue with the beam and scattered particle chambers is being able to know the geometry of the chambers and position them so that scattering angle offsets can be determined to better than 1 mr. In our view, this problem is largely a machining problem. If we keep the placement of wire chambers in a compact design around the target, a support structure can be machined so that the wire chambers are all positioned to about $10 \mu\text{m}$ over distances of several tens of cm, so that in principle angle offsets are below $100 \mu\text{r}$. This relies on a similar precision in the construction of the chambers.

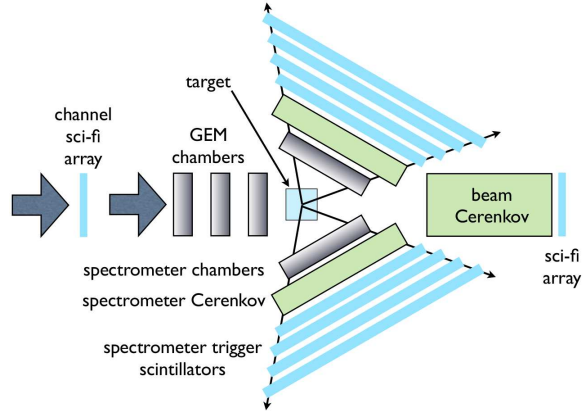


FIG. 14. A cartoon of the experimental setup.

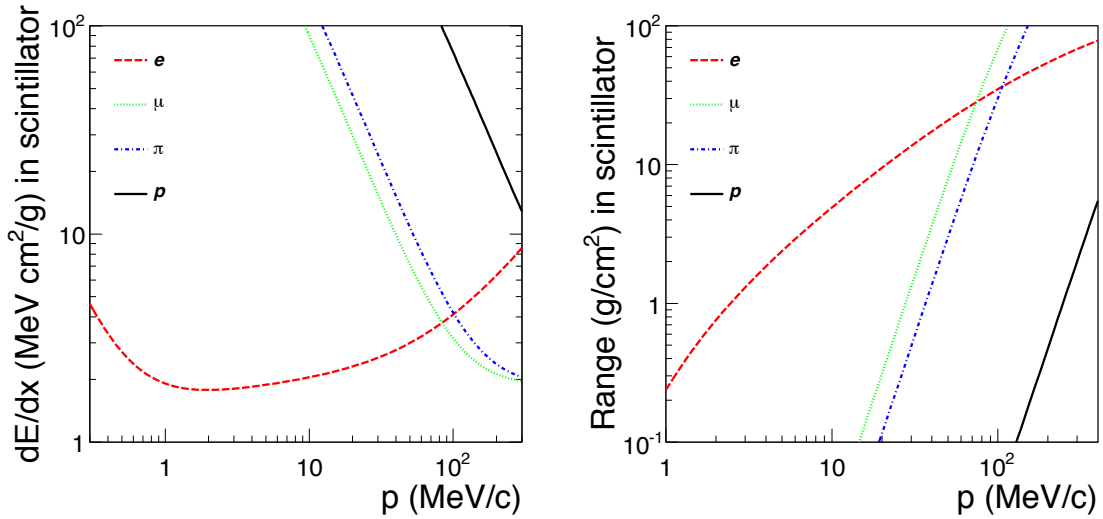


FIG. 15. Left: dE/dx in scintillator. Right: Range of particles in scintillator.

The simplest geometry for constructing the chambers is a rectangular box. If positioned 20 to 30 cm from the center of the target, the chamber areas would be moderately small, about 40 cm \times 35 cm to 60 cm \times 50 cm. To ensure efficient determination of tracks with good resolution, it is necessary to have at least 4 wire planes in each direction. Assuming a conventional chamber with a modest resolution of 0.2 mm, having the planes spread out over about a 10 cm distance would give about 3 mr angle determination, which is sufficient.

Scattered particle scintillators provide triggering, RF time determination, and particle identification. The scintillators will be the outermost elements in the detector stack. Positioning scintillator bars from 70 - 100 cm from the target requires bars that are about 1.4 - 2 m long. We plan 4 scintillator layers to allow a loose, highly efficient trigger. Each layer will consist of 16 paddles that are constant in scattering angle coverage from layer to layer, to simplify trigger logic and provide a rough trajectory. Note that the scintillators do not need to be positioned with the accuracy of the chambers, and an independent less-precise support system can be used for them.

Important considerations for the scintillator paddles are energy loss of particles passing through them and timing. Figure 15 shows dE/dx in polystyrene scintillator calculated from NIST ESTAR [42] for the electrons and NIST PSTAR [43] for protons. For pions and muons, we take dE/dx to be the same as for protons at the same $\beta\gamma$. Except for protons, all particles in the $\approx 100 - 200$ MeV/ c range of interest are close to minimum ionizing. Because dE/dx increases with momentum for the electrons, but decreases with momentum for the π 's and μ 's, it might be possible to use energy loss at the analysis level for some indication of particle type, but this will be difficult as fluctuations in dE/dx are large. Figure 15 also shows that the < 3 MeV/ c electrons present over much of the angle range stop in 1 g/cm² of scintillator the first layer of a multilayer scintillator trigger. Stopping 10 MeV/ c Moller or Bhabha electrons requires about 4 cm of scintillator. At this point it does not appear that there is any benefit to adding in an absorber for the forward angles, 20° - 30°, where these electrons appear, but we will study the issue further.

The second key feature of the scintillators is precise timing. The So. Carolina group has recently built scintillators 6 cm \times 6 cm by up to 2 m long for the Hall B / CLAS 12-GeV upgrade project. These scintillators have 56 ps (σ) resolution, at the analysis level rather than in hardware, with shorter bars having better resolution. With this resolution, the RF time determined by the scattered particle scintillators resolves the scattered particle types by about 4 ns / 56 ps = 70 σ at the analysis level. Thus, given such paddles and fast TDCs, in the analysis particle identification based on time of flight is sufficient in itself. RF timing of the scattered particles provides much more than adequate particle identification by itself. However, the several ns variation in timing as light propagates along a 1.4 - 2 m long scintillator paddle prevents determination of a useful RF time at the trigger level from these scintillators.

The addition of a Cerenkov detector to the detector stack provides a redundant and simple alternative means of particle identification available at the trigger level, in addition to the RF time determination from the beam sci-fi array. The most cost effective alternative appears to be a simple threshold Cerenkov counter for this experiment that would fire on e 's and μ 's, but not π 's. The intent would be to read out all events in which the Cerenkov fired (e 's and μ 's) and a prescaled fraction in which the Cerenkov had no signal (π 's) to maintain a low trigger rate while providing tests of efficiency.

One issue with using a threshold Cerenkov is that we will have to change the Cerenkov medium for the different incident momenta. However, a single medium can be used, with care, across much of the angle range for each incident momenta. Figure 16 shows the threshold n for a Cerenkov to fire for π 's and μ 's as a function of angle, for the three incident beam momenta. For the $p_{in} = 115$ MeV/ c setting, a Cerenkov with $n \approx 1.5 - 1.58$ would fire for μ 's but not π 's; possible materials include lucite with $n = 1.49$, crown glass with $n = 1.52$, and quartz with $n = 1.544$. (Due to the much lower π rate at 115 MeV/ c , the Cerenkov is not as important at this beam momentum.) For the $p_{in} = 153$ MeV/ c setting, a Cerenkov with $n \approx 1.32 - 1.36$ would fire for μ 's but not π 's; water has $n = 1.33$. For the $p_{in} = 210$ MeV/ c setting, a Cerenkov with $n \approx 1.19 - 1.2$ would fire for μ 's but not π 's; polycarbonate has $n = 1.20$.

Because of the variation of momenta with angle, a threshold Cerenkov will either be inefficient for accepting near threshold back angle muons or inefficient for rejecting forward angle π 's just about threshold. Figure 16 also shows the number of photons one could expect for a water Cerenkov detector per cm of thickness. From Fig. 12 one can see that at $p_{in} = 153$ MeV/ c the scattered π and μ momenta range from about 120 - 150 MeV/ c . While π 's do not fire the Cerenkov, it is also inefficient for detecting the largest angle μ 's. Thus the Cerenkov should only be used to limit triggers from more forward-angle π 's.

To summarize, the needed angle precision and resolution can be achieved with precise positioning of conventional wire chambers. Trigger scintillators can provide high efficiency for triggering and precise RF timing, more than sufficient for particle identification at the analysis level. We plan to use Cerenkov detectors to reduce the number of π triggers, supplementing what we will do with the beam sci-fi array RF timing.

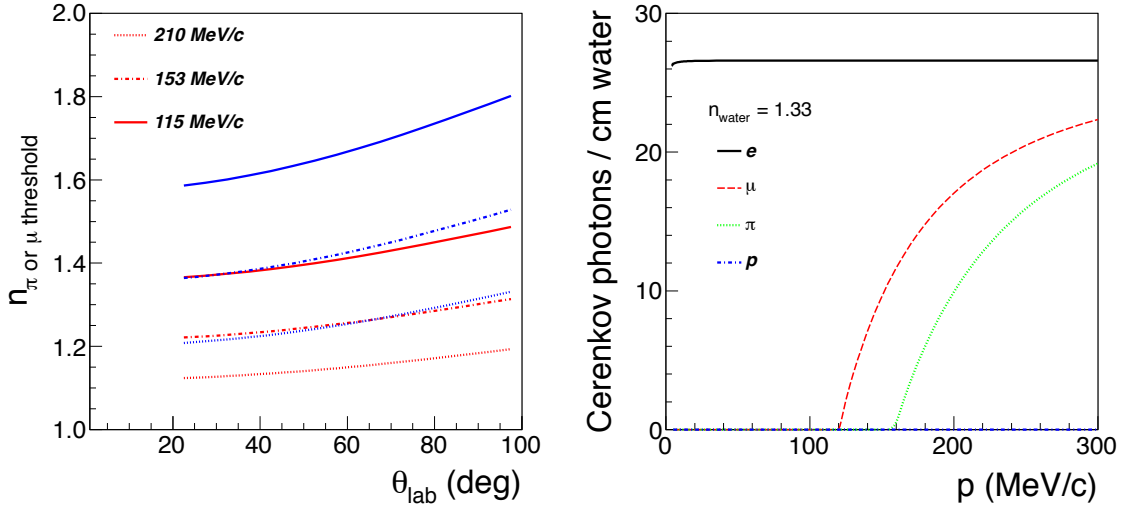


FIG. 16. Left: Threshold n for a Cerenkov to fire for π s (blue) and μ s (red) as a function of angle, for the three incident beam momenta. Right: Number of Cerenkov photons per cm of water as a function of particle momentum.

Pion and Muon decays

An aspect of the experiment not previously discussed is that the beam μ 's and π 's are unstable particles with lifetimes of $\approx 2.2 \mu\text{s}$ and 26 ns, respectively, that decay in flight. We argue here that the corrections for decays are small and precisely calculable, so the decays are not a significant issue.

The decay of 150 MeV/c π 's leads to a decay cone of 120 MeV/c μ 's at angle of about 14° from the pion direction. With $\beta_{\pi} \approx 0.75$, about 11% of the π 's will decay every meter. The decay muons do not go into the detectors appearing to come from the target, except for the very small probability that the π decays near the target and the μ scatters from the target into the detectors. Since the RF time for the decay muon is basically consistent with the π RF time, the event is identified as a π event. Thus, π decay is not a problem, as it does not lead to events identified as μ or e scattering events.

There are several corrections related to the decay of muons, all of which are small. For 150 MeV/c μ 's, $\beta_{\mu} \approx 0.8$ and about 0.1% of the muons decay per meter of flight path. The decay electrons typically come out in a cone at about 35° relative to the μ direction with a momentum of about 90 MeV/c. The first correction is that the flux of muons through the target is not the same as the flux of muons counted in the beam sci-fi arrays. The second correction is that about 0.1% of the scattered μ 's decay as they pass to and through the detector stack. A simulation taking into account the detector geometry will be needed to evaluate the correction. Third, about 0.004% of the muons in the beam decay in the region of the target. These events will appear to be muons based on RF time in the beam, but will form a peak in RF time in the detector stack about 0.8 ns offset from the μ RF time. If there is adequate resolution, they will also appear to be electrons based on dE/dx and the number of photons from the Cerenkov. Thus these events also can be well modeled and directly subtracted. We expect the uncertainty in the corrections for muon decays to be small compared to 0.1%.

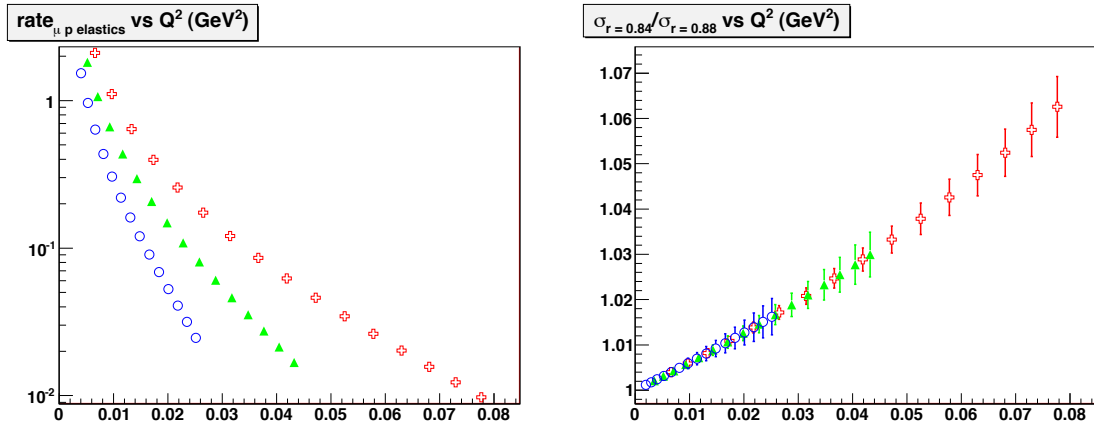


FIG. 17. Left: estimated count rates for μp elastic scattering for the conditions described in the text. Squares are for the 210 MeV/c data, triangles are for the 153 MeV/c data, and circles are for the 115 MeV/c data. Right: Projected cross sections with uncertainties for 30 day runs at each beam momentum. Points are the same as in left panel. For simplicity, we show the data all lying on the curve expected if the form factor is linear and reflects an rms radius of 0.84 fm, divided by the similar projection for a radius of 0.88 fm. Note that since the form factor ratio is taken to be linear, the cross section ratio is quadratic. But the approximation that $G_E = 1Q^2r^2/6$ starts to fail in the Mainz data around 0.02 GeV², as shown in Fig. 3.

Cosmic Rays

Because the rates of scattered particle events are low and the beam is nearly continuous, cosmic rays leading to showers might generate a significant trigger rate, if cosmic rays can generate triggers. As the trigger and the event analysis involve signals in both the spectrometer scintillators and beam sci-fi arrays, and the sci-fi array in the beam channel is remote from the detector stacks and shielded, cosmic rays are not expected to be a problem. Cosmic rays would also be rejected in the analysis because they form a smooth background in RF time, they do not typically generate tracks in the chambers that point to the target, and they do not typically have the timing through the scintillators of events coming from the target. The probability of cosmic ray background in an event is of order 10^{-5} .

Rates

We calculate μp elastic scattering rates assuming the beam fluxes shown in Table I, with the μ^+ flux at 210 MeV/c reduced to 1.4 MHz to reflect limiting the total flux to 20 MHz. The target is assumed to be 0.3 g/cm² of hydrogen. We assume 30 day runs at each energy, and neglect inefficiencies from detectors, triggers, computer dead time, or event analysis. We also neglect subtraction of background from the cell walls. Putting $\approx 3\sigma$ cuts on the cell walls has the effect of reducing the effective target length 6 mm out of 40 mm, or 15%. The residual cell wall rate will then be small and will have little effect on the uncertainties. The detectors are assumed to cover 50% of the 2π azimuthal angle range. The scattering angle range is 20° - 100°, and for display we sum the data with 5° bins and plot at the central Q^2 of each bin.

Figure 17 shows the resulting count rates and uncertainties for positive polarity beam at the three incident momenta. The μ^+p elastic scattering rates are modest, and require a moderately long run to bring the level of the uncertainties down towards the levels achieved in the Mainz experiment. The sub-1% statistical uncertainties we are attempting to achieve here are several

time better than the typical several percent μp scattering experiments discussed above.

With negative polarity, the μ^- rate is reduced around an order of magnitude, so uncertainties will increase about a factor of 3; this should be sufficient for a 2γ -exchange test over the range of the experiment. For this measurement, it should also be possible to rebin the data into a few higher statistics bins since the effect should vary slowly over the Q^2 range of the measurement.

The e^+p rates are as much as four times larger than the μ^+p rates, and the e^- rates are an order of magnitude larger than the μ^- rates. Thus, the statistics for comparing μp to ep will be no worse than $\sqrt{2}$ times the μ^+ uncertainties. The 2γ -exchange test on e 's will be at least a factor of three better than the test on μ 's.

Trigger

The experiment goal is to efficiently read out scattered μ 's and e 's in the angle range $20^\circ < \theta < 100^\circ$, of momentum greater than about 100 MeV/ c – the rate of such triggers is quite modest, at the level of a few tens of Hz. Lower momentum electrons will result from scattering from atomic electrons, but as discussed in relation to Fig. 15, the lower momentum e 's will be stopped in the initial layer of scintillator and will not generate triggers.

The main issue for the trigger is the hadronic scattering of π 's. The incident π flux ranges from an order of magnitude smaller than the e and μ flux at 115 MeV/ c , to about equal at 153 MeV/ c , to an order of magnitude larger at 210 MeV/ c . Hadronic scattering is roughly two orders of magnitude larger than electromagnetic scattering, so the scattered π rate ranges from about $10 - 10^3$ times larger than the scattered $e + \mu$ rate.

Triggers from the larger rate of scattered pions only need to be suppressed at a level consistent with keeping DAQ dead time low. This corresponds to a factor of about 100 suppression for the worst kinematics, positive polarity at $p_{in} = 210$ MeV/ c . At this momentum, the RF times are nearly 6 ns apart. We expect to be able to achieve time resolution with an RMS width about 1 ns with the beam counters. A cut about halfway between the π and μ RF times would only reject 0.1% of the μ 's, and allow through into the DAQ about equal numbers of π 's and μ 's, leading to a very manageable DAQ rate. (We expect to make the cut somewhat looser to reject fewer μ 's while accepting more π 's. The π 's are easily rejected at the analysis stage and widening the cut reduces the systematic correction for inefficiency.) At present we do not see an issue with implementing this capability with the FPGA system being developed. As indicated above, we are also considering requiring a Cerenkov signal to be present for the normal trigger for events scattering at more forward angles, and prescaling readout of events for which a Cerenkov signal is not present.

Systematic Uncertainties

The systematic uncertainties have largely been discussed above, and are summarized and estimated in Table II. The most important systematics concern the knowledge of angles. Since there is no strong magnetic field used to momentum analyze particles in the detector system, knowledge of angles largely comes down to an issue of mechanical design, so that wire chambers are precisely constructed and positioned. The systematic related to the multiple scattering averaging over angle, shown in Fig. 10, can be reduced by correcting for this effect; the correction relies on knowing material thicknesses to calculate the multiple scattering, but is insensitive to the form factors as the effect arises largely from the Mott cross section.

The 2γ correction remains a potential concern, but a goal of the experiment is to measure – or at least constrain – it.

In addition to the usual estimates and internal checks of systematic uncertainties, the measurement of elastic ep scattering allows a direct comparison to world ep data and fits, providing

TABLE II. Estimated experimental systematics for μp elastic scattering. Systematics for ep scattering are similar, except for radiative corrections which are about 4 times larger. For systematics that vary with angle, a typical value for $\theta = 50^\circ$ is given.

Systematic Uncertainty	Absolute (%)	Point-to-point (%)
$x\rho_{target}$	1.0	-
Beam flux ($\pi / \mu / e$ misidentification)	small	-
Radiative correction	0.3	0.1
Solid angle	0.2	0.2
Efficiencies - triggering, analysis, etc.	0.5	0.1
Beam energy	0.2	0.1
Averaging over beam energies	small	small
Knowledge of angle	0.45	0.3
Averaging over angles / multiple scattering	0.2	0.2
Cell wall subtraction	small	small
Cosmic ray subtraction	small	small
π / μ decay corrections	small	small
TOTAL	1.3	0.5

a measure of the systematic uncertainties. We are also considering whether it makes sense to measure $^{12}\text{C}(e, e')$ elastic scattering at a single setting, 153 MeV/c, for comparison to world data.

The systematics shown in Table II are appropriate for comparing data sets, if we are comparing ep and μp data at the same time, there is a further reduction in the experimental systematics. Because of kinematic differences, the same Q^2 is not at the same angle for the two reactions, as shown in Fig. 12, but the systematics for energy and angle offsets and averaging are very similar for the two reactions, so these effects largely cancel when comparing ep and μp data measured simultaneously. The systematics of misidentified particles, radiative corrections, and detector efficiencies will be slightly different for the two particle types.

Test Run

We have concluded that this experiment cannot generally be carried out with existing equipment; it will require that the proponents construct new equipment for nearly all aspects of the experiment. To ensure the success of the experiment, we request time to carry out a test measurement with existing GEM chambers, scintillators, and foil targets. The goal is not to measure a cross section, but to ensure that the beam composition, emittance and backgrounds are well understood so that the new equipment will be constructed appropriately for the cross section measurement to succeed. We plan to run the test measurement largely at $p_{in} \approx 153$ MeV/c, but the other momenta and both polarities are needed as well to check the beam composition. We expect the test measurement to take a few months to set up in the Hall, with a few weeks of beam time needed to carry out the measurements.

COLLABORATION RESPONSIBILITIES AND COMMITMENTS NEEDED FROM PSI

Because of the need to construct new equipment, it will be necessary to submit funding proposals for the second stage of the experiment. Members of the collaboration are working on applications for European Research Council Advanced Grant (proposals due February 2012), and planning on submitting applications for U.S. Department of Energy and National Science Foundation grants (proposals due fall 2012). These grants would result in money being available in 2013, and new equipment being available in 2013-2014. This limits the start of the full experiment to be no sooner

TABLE III. Task list.

Task	Responsible
Channel tune	PSI
Channel intermediate focal point detectors	MIT, Tel Aviv
Beam sci-fi arrays	Rutgers
Beam GEM chambers	Virginia
Beam Cerenkov detector	Temple
Foil targets	Jerusalem
LH ₂ target	PSI, Rutgers
Scattered particle chambers	MIT, Tel Aviv
Scattered particle scintillator paddles	South Carolina, Tel Aviv
Scattered particle Cerenkov	Jerusalem
Trigger	Rutgers
DAQ design and implementation	PSI, Rutgers
Radiative corrections	Temple
Analysis issues	Argonne
Ph.D. students	Jerusalem, MIT, Tel Aviv U.
People on site (besides Ph.D. students) for extended period	Jerusalem, MIT, Rutgers, Tel Aviv

than late 2014.

At present various collaboration members are studying and considering constructing various aspects of the experiment. A number of these tasks are given in Table III. Responsibility for tasks might change based on available funding. We are also considering whether it would make sense to have a staging area for pre-assembly of the experimental equipment at Tel Aviv or Jerusalem, rather than at PSI.

The experiment will likely require 3 - 6 months to assemble and debug / commission at PSI before production data taking starts. It might be more efficient for parts of the experimental equipment to be debugged / commissioned with a few days of beam before the entire experimental setup is complete.

There are several commitments we will need from PSI to make the experiment possible, and several contributions that could make the experiment easier.

We will need access to the PSI π M1 area over a period of approximately 3 years. The first year, mid 2012-2013, will be for installation of a test setup and limited beam and test cross section measurements intended to ensure a successful experiment. We do not expect to need access to the π M1 area during the second year, 2013 - 2014. We anticipate bringing equipment to the π M1 area starting about mid 2014, with the experiment running from late 2014 or early 2015 through the middle of 2015. Ideally there will be an initial lower intensity commissioning phase and 1 month of production running, followed by a few month analysis period to ensure the quality of the data, before the bulk of the production running.

We request that PSI host a technical review of the proposal. Having a technical review approximately mid to late summer 2012, with results available by September 2012, would put us in a stronger position for requesting funding from U.S. funding agencies or others subsequently.

Operation of the equipment requires that PSI provide infrastructure, including the π M1 area, counting house / office space area, and access to power and computer networks.

Installation of detectors in the intermediate focal point of the π M1 beamline will require PSI assistance in design and engineering and probably installation by PSI technical people.

Installation of equipment within the π M1 beamline area will require technical support, including craning and surveying.

SAFETY ISSUES

The proposed experiment makes use of detectors and targets that are common to subatomic physics experiments. At this point we do not have a detailed system design, so we only briefly review common safety issues for these systems. We do not consider beam-related safety concerns as the π M1 area and its safety systems have been operational for many years.

Cryotarget: Standard low power cryotargets involve several liters of liquid hydrogen at a temperature of about 20 K in a cell with thin walls, typically encased in a vacuum system. The main potential issue is a rupture of the cell and vacuum system. Rupture of a vacuum system can generate a loud sound that can damage hearing; warning signs, roped off areas, and ear protection for those who must work near the system are a standard counter measures. If the target ruptures the hydrogen liquid expands in volume about three orders of magnitude and quickly rises through the air. This presents potential oxygen deficiency hazards and potential damage to exposed skin or eyes. We believe that the size of the building containing the π M1 area and the quick rise of the lighter than air hydrogen mitigate any potential ODH hazard. Damage to skin and skins is limited by protective clothing including eye protection.

Low Current, High Voltage: Wire chambers and phototubes operate with few kV DC power, which could if shorted provide a power source to ignite a fire or harm a person either directly or through surprise and an ensuing accident. All HV is shielded so that it cannot be directly accessed, and supplied by power supplies with trip limits set, so that any shorting of the supply leads to the supply turning off.

High Current, Low Voltage: Numerous electronics modules require power supplied at low voltage, perhaps 5 V, but at large currents, often many hundreds of amps for the entire experiment. Chamber mounted readout electronics are one example of this; electronics modules mounted in VME or NIM crates are another example. Because of the high current capabilities, shorts to ground might lead to exploding wires, fires, or personal injury if, e.g., the short is through jewelry worn by a person. Standard safety techniques include having no exposed contacts and fuses.

Chamber Gas: Wire chambers are operated with various gas mixtures typically supplied from high pressure gas cylinders. There are well established gas cylinder safety procedures since in accidents gas cylinders can quickly become very effective missiles. The ODH hazard is minimal as it is unlikely that a large amount of gas would be released into a small part of the M1 area. A more common concern is that many gas mixtures are in principle flammable if sufficiently concentrated with the oxygen in air, and must be kept from an ignition source, such as a spark of flame. It is common in this case to analyze for the area the maximal leak rate permitted for the chamber systems, and monitor system leak rates. In the case of the π M1 area, it is likely that the chamber gas use is so small given the building containing the area that even venting the used chamber gas directly into the area does not cause a flammable gas hazard. The GEM chambers have been operated in the past with a non-flammable mixture, 70% Argon and 30% CO₂, but we have not at this time specified the gas mix for the chambers for tracking scattered particles.

Mechanical Issues: The detector systems are heavy in total and require properly designed and constructed support structures. Assembly of the apparatus is likely to require a crane; there are standard safety procedures for crane use. Accessing some of the higher detector elements might involve use of a ladder or platform, which might further lead to fall protection issues. Again, there are well developed safety procedures in these cases that must be designed into the system constructed.

SUMMARY

About 1.5 years after the radius of muonic hydrogen was found to be 5σ inconsistent with earlier determinations from atomic hydrogen level transitions and ep elastic scattering, no resolution to the puzzle has been found. We repeat the quote from the Jefferson Lab PAC: “*Testing of this*

result is among the most timely and important measurements in physics.”

We propose to measure μ^\pm and e^\pm elastic scattering, at the same time with the same equipment, which will allow a second determination of the consistency of the μp interaction with the ep interaction, as well as a test of the importance of 2γ exchange effects. The experiment has the potential to demonstrate that the μp and ep interactions are different, violating universality, by measuring at higher precision than previous scattering tests. The experiment is technically feasible on a time scale of about 3 years.

-
- [1] P.J. Mohr, B.N. Taylor, and D.B. Newell, *Rev. Mod. Phys.* **80**, 633 (2008).
 - [2] I. Sick, *Phys. Lett. B* **576**, 62 (2003).
 - [3] R. Pohl *et al.*, *Nature* **466**, 213 (2010).
 - [4] J. Bernauer *et al.*, *Phys. Rev. Lett.* **105**, 242001 (2010).
 - [5] X. Zhan *et al.*, *Phys. Lett. B* **705**, 59 (2011).
 - [6] B. Batell, D. McKeen, and M. Pospelov, arXiv:1103.0721.
 - [7] V. Barger, C.W. Chiang, W.Y. Keung, and D. Marfatia, arXiv:1109.6652.
 - [8] G.A. Miller, A.W. Thomas, J.D. Carroll, and J. Rafelski, *Phys. Rev. A* **84**, 020101(R) (2011).
 - [9] J. D. Carroll, A. W. Thomas, J. Rafelski and G. A. Miller, *Phys. Rev. A* **84**, 012506 (2011) [arXiv:1104.2971 [physics.atom-ph]].
 - [10] J. D. Carroll, A. W. Thomas, J. Rafelski and G. A. Miller, *AIP Conf. Proc.* **1354**, 25 (2011) [arXiv:1105.2384 [physics.atom-ph]].
 - [11] G.A. Miller, private communication.
 - [12] A. De Rújula, *Phys. Lett. B* **693**, 555 (2010).
 - [13] A. De Rújula, *Phys. Lett. B* **697**, 26 (2011).
 - [14] I.C. Clöet and G.A. Miller, *Phys. Rev. C* **83**, 012261 (2011).
 - [15] M.O. Distler, J.C. Bernauer, and T. Walcher, *Phys. Lett. B* **696**, 343 (2011).
 - [16] B.Y. Wu and C.W. Kao, arXiv:1108.2968.
 - [17] C. E. Carlson and M. Vanderhaeghen, arXiv:1109.3779 [physics.atom-ph].
 - [18] G. Paz, arXiv:1109.5708.
 - [19] L.S. Cardman *et al.*, *Phys. Lett. B* **91**, 203 (1980).
 - [20] E.A.J.M. Offermann *et al.*, *Phys. Rev. C* **44**, 1096 (1991).
 - [21] L.A. Schaller *et al.*, *Nucl. Phys. A* **379**, 523 (1982).
 - [22] W. Ruckstuhl *et al.*, *Nucl. Phys. A* **430**, 685 (1984).
 - [23] R.W. Ellsworth *et al.*, *Phys. Rev.* **165**, 1449 (1968).
 - [24] J. J. Kelly, *Phys. Rev. C* **70**, 068202 (2004).
 - [25] L. Camilleri *et al.*, *Phys. Rev. Lett.* **23**, 153 (1969).
 - [26] I. Kostoulas *et al.*, *Phys. Rev. Lett.* **32**, 489 (1974).
 - [27] A. Entenberg *et al.*, *Phys. Rev. Lett.* **32**, 486 (1974).
 - [28] L. Camilleri *et al.*, *Phys. Rev. Lett.* **23**, 149 (1969).
 - [29] V. Tvaskis, *et al.*, *Phys. Rev. C* **73**, 025206 (2006).
 - [30] J. Arrington *et al.*, “A Measurement of Two-Photon Exchange in Unpolarized Elastic Electron-Proton Scattering,” Jefferson Lab experiment 05-017.
 - [31] A. Gasparian *et al.*, Jefferson Lab PAC38 proposal PR-11-1xx, unpublished.
 - [32] R. Gilman, unpublished.
 - [33] G. Ron, E. Piassetzky, and B. Wojtsekhowski, *JINST* **4**, P05005 (2009).
 - [34] M. Mezziane *et al.*, *Phys. Rev. Lett.* **106**, 132501 (2011).
 - [35] T. Averett *et al.*, Jefferson Lab Experiment E05-015, unpublished.
 - [36] A. Afanasev *et al.*, Jefferson Lab Experiment E07-005, unpublished.
 - [37] N. Akopov *et al.*, OLYMPUS Collaboration, <http://web.mit.edu/OLYMPUS/index.html>.
 - [38] See, e.g., A.V. Gramolin *et al.*, arXiv:1112.5369.
 - [39] J.P. Albanese *et al.*, *Nucl. Instrum. Methods* **158**, 363 (1979).
 - [40] C. Casella *et al.*, *Design and Performance of the FAST Detector*, submitted to NIM (2011).
 - [41] http://aea.web.psi.ch/beam2lines/beam_pim1.html.
 - [42] Electron ranges were calculated with the NIST ESTAR database at <http://physics.nist.gov/PhysRefData/Star/Text/ESTAR.html>.
 - [43] Proton ranges were calculated with the NIST PSTAR database at <http://physics.nist.gov/>

`PhysRefData/Star/Text/PSTAR.html`.

[44] W. Lorenzon, private communication.